PERGAMON

International Journal of Heat and Mass Transfer 46 (2003) 457–468

International Journal of HEAT and MASS TRANSFER

www.elsevier.com/locate/ijhmt

Gas absorption into "string-of-beads" liquid flow with chemical reaction: application to carbon dioxide separation

Kazunori Uchiyama [1], Hirofumi Migita [2], Ryo Ohmura [3], Yasuhiko H. Mori *

Department of Mechanical Engineering, Keio University, 3-14-1 Hiyoshi, Kohoku-ku, Yokohama 223-8522, Japan

Received 30 November 2001; received in revised form 19 July 2002

Abstract

This study examines the performance of "string-of-beads" liquid flow on vertical wires as a novel gas–liquid contact device for gas absorption using a chemically reacting liquid absorbent. The string-of-beads flow is a distinct on-wire liquid-flow pattern consisting of annular thin liquid films sheathing a wire and teardrop-shaped liquid beads alternately aligned on the wire at regular intervals. We have performed experiments of CO_2 absorption by an aqueous monoethanolamine solution in string-of-beads flow on a single wire and have developed an analytic gas-absorption model relevant to the experiments. The model well simulates the CO_2-absorption characteristics observed in the experiments, thereby suggesting the utility of the model in predicting the chemical gas-absorption performance of multiple-wire gas–liquid contactors.

1. Introduction

The efficiency of gas absorption into a liquid absorbent is strongly dependent on the geometrical and hydrodynamic design of a particular gas–liquid contactor. In fact, conventional contactor designs such as wetted-wall and packed-bed columns are not well suited for processing a huge amounts of industrial waste gases due to inevitable insufficient contact-area-to-volume ratios or large gas-side pressure losses during operation. For example, separating carbon dioxide (CO_2) from flue gases exhausted by fossil-fuel-fired power plants, a potential measure to mitigate the human-originated greenhouse effect, requires use of a gas–liquid contact device that efficiently removes CO_2 from a flue-gas flow at an enormously high rate without imposing on the flow such a substantial pressure loss as to necessitate the addition of a flue-gas compression process. Accordingly, use of *wetted-wire columns* for processing flue gases or other industrial waste gases is considered to be more advantageous than that of conventional types of gas–liquid contactors including spray, wetted-wall, and packed-bed columns, where *wetted-wire columns* refers to vertical columns each equipped with internal multiple wires vertically hung such that a liquid absorbent flows downward on the wires while contacting countercurrent gas flow.

Providing the wires are well wetted with a particular liquid absorbent, controlling its flow rate on each wire within a prescribed range produces the flow referred to as "string-of-beads" flow. That is, a distinctive on-wire liquid-flow pattern occurs, one consisting of annular thin liquid films sheathing a wire and teardrop-shaped liquid beads alternately aligned on the wire at regular intervals [1]. The beads slide down the wire at a constant

* Corresponding author. Tel.: +81-45-566-1522; fax: +81-45-566-1495.

E-mail address: yhmori@mech.keio.ac.jp (Y.H. Mori).

[1] Present address: Nippon Soken, Inc., 14 Iwaya, Shimohasumi-cho, Nishio-shi, Aichi-ken 445-0012, Japan.

[2] Present address: Hitachi Construction Machinery Co., Ltd., 650 Kandatsu-cho, Tsuchiura-shi, Ibaraki-ken 300-0013, Japan.

[3] Present address: Institute for Energy Utilization, National Institute of Advanced Industrial Science and Technology (AIST), 2-17-2-1 Tsukisamu-Higashi, Toyohira-ku, Sapporo 062-8517, Japan.

0017-9310/03/$ - see front matter
PII: S0017-9310(02)00301-0

Nomenclature

a	d_f/d_w
A_d	surface area of liquid bead
A_n	dimensionless constants ($n = 1, 2, \ldots$) used in Eq. (8)
c, c_s	mass concentration and mass-based physical solubility, respectively, of CO_2 in liquid absorbent
$\tilde{c}$, $\tilde{c}_s$	molar concentration and mole-based physical solubility, respectively, of CO_2 in liquid absorbent
$\tilde{c}_d$, $\tilde{c}_f$	mixed-mean values of $\tilde{c}$ in bead and film, respectively
$\hat{c}$	mass of CO_2 absorbed in unit volume of liquid absorbent
$\hat{c}_{sat}$	mass-based overall solubility of CO_2 in liquid absorbent
$\widetilde{C}$	molar concentration of monoethanolamine in liquid absorbent
$\widetilde{C}_d$, $\widetilde{C}_f$	mixed-mean values of $\widetilde{C}$ in bead and film, respectively
$\widetilde{C}_L$	time-averaged, mixed-mean value of $\widetilde{C}$ at arbitrary axial location
d_d	diameter of liquid bead assumed to be spherical (approximated by $(d_{d1}d_{d2}^2)^{1/3}$)
d_{d1}, d_{d2}	axial length and maximum diameter, respectively, of liquid bead
d_f	diameter of cylindrical liquid film
d_n	inside diameter of nozzle
d_w	wire diameter
D	diffusivity of CO_2 in liquid absorbent
E	liquid-side mass transfer efficiency
g	acceleration due to gravity
k, k'	reaction rate constants defined by Eqs. (4) and (5), respectively
K_R	dimensionless first-order reaction constant defined in Section 3.3.2
L_d	axial interval between successive beads
$\dot{M}$	rate of mass transfer from gas flow into liquid absorbent
r	CO_2–monoethanolamine reaction rate defined as the molar rate of loss of CO_2 per unit volume of liquid absorbent
R_d, R_f, R_G	thermal resistances defined as β_d^{-1}, β_f^{-1} and β_G^{-1}, respectively
S_f	cross-sectional area of liquid film
Sh_d	Sherwood number defined as $\beta_d d_d/D$
t	time
U_d, U_f	fall velocity of bead and average flow velocity in film, respectively
V_d	bead volume
$\dot{V}_L$	volume flow rate of liquid absorbent
x	vertical distance measured downward from nozzle tip

Greek symbols

β_d	mass transfer coefficient inside liquid bead
β_f	mass transfer coefficient inside liquid film
β_G	gas-phase-side local mass transfer coefficient
ν_L	kinematic viscosity of liquid absorbent
λ_n	dimensionless constants ($n = 1, 2, \ldots$) used in Eq. (8)
τ	time interval of successive falls of liquid beads
τ_d	dimensionless time defined in Section 3.3.2
τ_{fg}	period of film-reforming cycle

Subscripts

in, 0	condition of liquid absorbent before contact with gas flow
out	condition of liquid absorbent after contact with gas flow

velocity substantially higher than the flow velocity of the films such that continuous bead-to-film and film-to-bead mass displacement presumably takes place in the liquid absorbent phase, which is thought to in turn reduce its diffusive resistance.

We first tested this hypothesis using a string-of-beads flow of water down a single glass wire placed in an upward flowing CO_2/N_2 mixture [2]. Physical absorption of CO_2 by the water was experimentally studied. Also developed was an analytic model that can predict the absorption using observational knowledge of configurations and motions of the beads and films. Experimental results were utilized in estimating gas-absorption performance of wetted-wire columns equipped with multiple wires, with findings showing application potential of such wetted-wire columns, i.e., their gas-absorption performance is comparable to that of conventional packed-bed columns, while the pressure loss imposed on gas flow in the wetted-wire columns is comparably much smaller.

Many industrial gas-absorption processes employ chemical absorbents having much larger absorption capacities than physical absorbents. Regarding the separation of CO_2 from gas mixtures, for example, aqueous solutions of various types of amines are expected to be effective absorbents. Here we extend our previous study on physical absorption by water in string-of-beads flow [2] by experimentally investigating the chemical ab-

sorption of CO_2 by a monoethanolamine (MEA) solution in the same flow pattern. An analytic model of chemical absorption is also described, one which not only assists in interpreting the experimental results, but also allows predicting the absorption performance of string-of-beads flows of chemical absorbents.

2. CO_2 absorption experiments

2.1. Apparatus and procedure

Fig. 1 shows the experimental setup used in the present experiments. This setup is slightly different from that described in our previous paper [2], and hence it is outlined only briefly, noting the specific changes made in performing the present experiments.

A CO_2/N_2 mixture adjusted to 0.1 mole fraction of CO_2 is supplied to the bottom of a vertically oriented cylindrical test column made of a transparent poly(methyl methacrylate) (PMMA) pipe (ID, 100 mm; length, 1000 mm). Upward flow occurs at a constant superficial velocity of 31.8 mm/s. A liquid absorbent, i.e., 15- or 30-wt.% aqueous MEA solution, is fed onto the top portion of a single "wire" positioned at center of the column such that its downward flow is countercurrent to the gas flow. The wire is actually a straight stainless-steel tube (OD, 0.88 ± 0.02 mm), being different than the fragile glass wire used previously [2]; this is because suitable wettability could be obtained, using the stainless-steel tube in conjunction with 15- and 30-wt.% MEA solutions. The top portion of the wire is inserted into a tubular nozzle such that the absorbent pumped by a non-pulsating plunger pump (Lab-Quatec Model 21MP-311P) flows out of the concentric annular space inside the nozzle onto the surface of the wire protruding out of the nozzle tip (Fig. 2). Absorbent reaching the bottom of the test column is drained out of the test column through a stainless-steel tubing that connects the central opening of the piston-like, vertically movable bottom plate to a three-way valve which allows a prescribed volume of the absorbent to be withdrawn into an airtight sampling vial when necessary. The amount of CO_2 absorbed in each absorbent sample is determined by the precipitation-titration method described by Jou et al. [3], i.e., using 0.1 kmol/m^3 aqueous $BaCl_2$ solution and methyl orange indicator in the precipitation and titration operations, respectively.

Experiments were carried out in a laboratory temperature-controlled at 25 ± 1 °C using test fluids

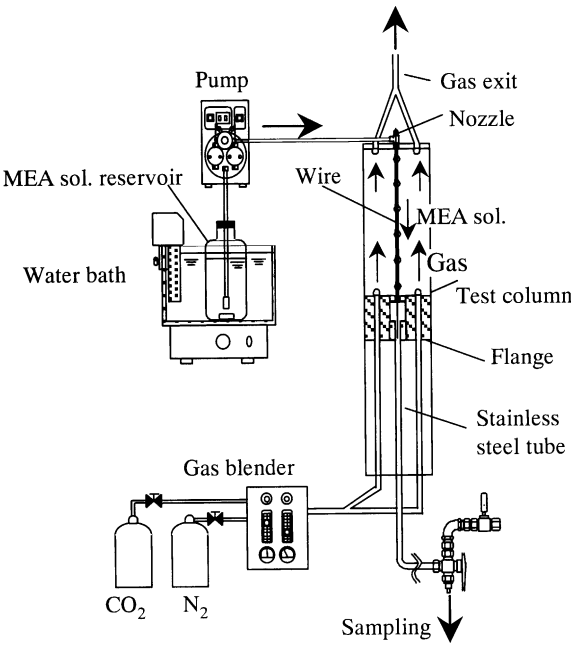

Fig. 1. Experimental setup.

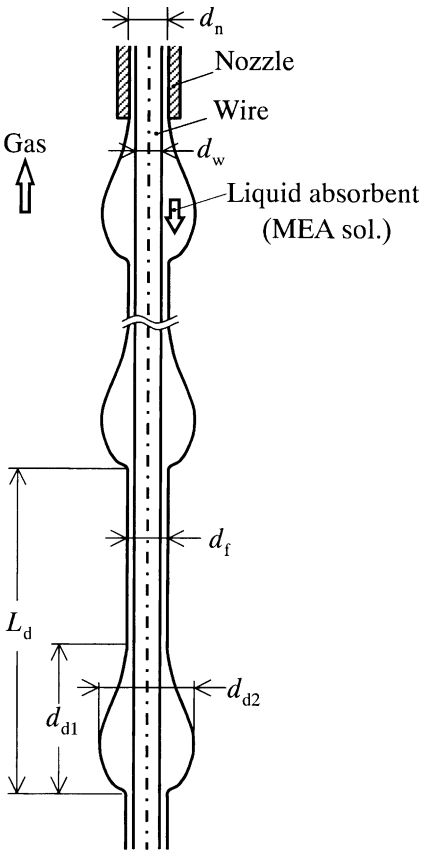

Fig. 2. Schematic illustration of nozzle–wire assembly and string-of-beads flow of liquid absorbent. Indicated in the illustration are geometrical quantities used for flow characterization.

thermally equilibrated with laboratory air. Full details of the experimental work is described by Uchiyama [4].

2.2. Absorbent properties and operational conditions

The properties of the employed absorbents, i.e., 15- and 30-wt.% aqueous MEA solutions, and of the CO_2-absorbent systems are summarized in Table 1. Many of these properties will be referred to later in this paper (particularly in Section 3). Here we should note that, regarding the mechanical properties of each solution relevant to its on-wire flow behavior, the only substantial difference between the two is in viscosity.

Using a stereomicroscope (Olympus SZ6045-TRCTV) connected to a high-speed video camera (Photron Fastcam-ultima-UV3), preliminary experiments were performed without the PMMA column enclosing the wire.

Table 1
Physical and chemical properties of aqueous MEA solutions and CO_2–MEA-solution systems at a temperature of 25 °C, a total pressure of 101.3 kPa, and a CO_2 partial pressure of 10.13 kPa

Property	15-wt.% MEA solution	30-wt.% MEA solution
Density ρ_L (kg/m^3)	1003[a]	1010[a]
Viscosity μ_L (mPa s)	1.45[b]	2.41[c]
Surface tension (mN/m)	59.1[d]	55.1[d]
Physical solubility of CO_2 c_s (kg/m^3)	0.119[e]	
Overall solubility of CO_2 $\hat{c}_{sat}$ (kg/m^3)	64.9[f]	127.6[g]
Diffusivity of CO_2 D (m^2/s)	1.42×10^{-9}[h]	
Reaction rate constant k (m^3/(mol-MEA s))	5.40[i]	

[a] Calculated by an empirical correlation given by Song et al. [5].
[b] Estimated by curve-fitting to experimental data of Hikita et al. [6].
[c] Estimated by extrapolating the curve fitted to experimental data of Hikita et al. [6].
[d] Estimated by curve-fitting to experimental data of Vázquez et al. [7].
[e] Estimated by using the N_2O analogy [8] to combine three empirical correlations given by Versteeg et al. [9], one for the solubility of N_2O in MEA solutions and the other two for Henry's constants for CO_2–water and N_2O–water systems, respectively.
[f] Estimated by curve-fitting to experimental data of Lee et al. [10] and of Muhlbauer and Monaghan [11].
[g] Estimated by curve-fitting to experimental data of Jou et al. [3].
[h] Estimated by using the N_2O analogy [12] to combine the value of CO_2–MEA-solution diffusivity read by curve-fitting to experimental data of Sada et al. [13] with empirical correlations for CO_2–water and N_2O–water diffusivities, respectively, both given by Versteeg et al. [8].
[i] Calculated by empirical correlation by Hikita et al. [14].

Analysis of obtained video images of the solutions in string-of-beads flow allowed us to determine the axial length d_{d1}, maximum diameter d_{d2}, axial interval L_d, and fall velocity U_d of the beads, as well as the cylindrical-film diameter d_f, at each level of the volume flow rate $\dot{V}_L$ of each solution flowing from the annular clearance inside each of two different-sized nozzles (ID, $d_n = 1.12$ and 1.25 mm) that were alternatively used. (Some details of determining d_{d1} are described in the Appendix A) Fig. 3 shows variations in d_f, d_{d2}, and U_d versus $\dot{V}_L$ for each solution/nozzle combination. The range of $\dot{V}_L$ covered by the data for each solution/nozzle combination almost corresponds with the full range for stable string-of-beads flow, i.e., that for flow pattern B defined by Hattori et al. [1]. Note that only U_d shows a large difference between the two solutions, being consistent with the large difference in viscosity between them (Table 1).

Table 2 lists the absorbent flow conditions used in the absorption experiments. The flow rate of the 15-wt.% MEA solution released from each nozzle was alternatively set at two different levels. The higher one was determined so as to maximize U_d while the lower one was set close to the lower border of the stable string-of-beads flow range. The flow rate of the 30-wt.% MEA solution was adjusted to that in corresponding experiments using the 15-wt.% solution.

2.3. Results and discussion

We employ two indices for evaluating the effectiveness of the gas-to-liquid CO_2 transfer, i.e., the mass-

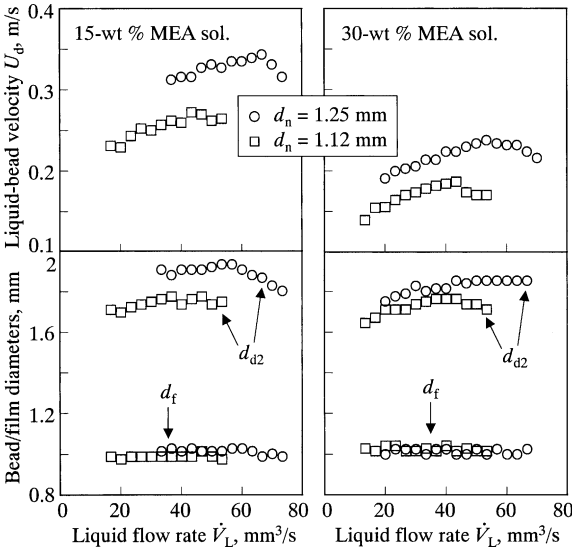

Fig. 3. Variations in fall velocity U_d and maximum diameter d_{d2} of beads and cylindrical-film diameter d_f with volume flow rate of liquid absorbent, $\dot{V}_L$, when a stainless-steel wire 0.88 mm in diameter was used together with each of the two tubular nozzles having different inside diameters, d_n.

Table 2
Flow rates of MEA solutions used in CO_2-absorption experiments

MEA concentration (wt.%)	Nozzle ID d_n (mm)	Flow rate $\dot{V}_L$ (mm^3/s)
15	1.12[a]	23.4, 40.1
15	1.25[a]	40.1, 66.8
30	1.12[a]	23.4, 40.1

[a] With tolerance $+0.04/-0.02$ mm.

based rate of CO_2 transfer, $\dot{M}$, and the liquid-side transfer efficiency, E, defined as

$$\dot{M} = (\hat{c}_{out} - \hat{c}_{in})\dot{V}_L, \tag{1}$$

$$E = \frac{\hat{c}_{out} - \hat{c}_{in}}{\hat{c}_{sat} - \hat{c}_{in}}, \tag{2}$$

where $\hat{c}$ denotes the mass of CO_2 absorbed into a unit volume of the MEA solution used (i.e., the sum of the mass of CO_2 reacted with MEA and that physically dissolved in the solution), subscripts "in" and "out" respectively indicate the MEA solution sampled before and after flowing down the wire in the test column, and "sat" denotes the saturation of the MEA solution with CO_2 under the partial pressure of CO_2 adjusted to one-tenth of 1 atm (101.3 kPa). The value of $\hat{c}_{sat}$, the solubility of CO_2 in the solution, is given in Table 1. Regarding $\hat{c}_{in}$, it was found to be negligibly small in all experiments.

The results of the experiments are summarized in Fig. 4 in the form of $\dot{M}$ and E plotted versus x, the vertical distance from the nozzle tip down to the upper surface of the bottom plate of the test column, i.e., the distance the MEA solutions flowed down the wire while being in contact with the gas mixture. Fig. 4(a) compares $\dot{M}$–x and E–x relations obtained with two different nozzles and different flow rates of the 15-wt.% MEA solution, while Fig. 4(b) shows corresponding results for both solutions used with the finer nozzle. Here we find that $\dot{M}$ increases with increasing $\dot{V}_L$, whereas the opposite occurs for E. An increase in $\dot{V}_L$ will presumably increase the frequency of bead formation such that a larger number of beads are aligned on the wire at smaller intervals L_d. More beads provides a larger gas–liquid interfacial area, while smaller L_d would shorten the *life* of each film-forming liquid element, i.e., the period of time after it is reformed at the rear of a particular bead until it is engulfed by the next-coming bead. Both the larger interfacial area and the faster cyclic reformation of film-forming liquid elements should contribute to increasing the rate of interphase CO_2 transfer. However, the increase in the rate of CO_2 transfer thus obtained is not to such an extent as to be proportional to an increase in $\dot{V}_L$. This is because the average velocity of the absorbent flowing down the wire increases with increasing $\dot{V}_L$, thereby shortening the residence time of the absorbent in the test column, which in turn tends to decrease the transfer efficiency E.

The effect of nozzle diameter d_n should also be noted (Fig. 4(a)) in that both $\dot{M}$ and E are improved for a finer nozzle (1.12 vs 1.25 mm). This effect is surmised to occur due to the nature of liquid-bead formation, i.e., absorbent issuing from a narrower clearance ($(d_n - d_w)/2 =$ 0.12 vs 0.19 mm) produces more frequent formation of smaller beads fall at lower velocity (Fig. 3).

The effect of the MEA concentration is similar to that of $\dot{V}_L$ in that a higher concentration produces an increase in $\dot{M}$ and decrease in E (Fig. 4(b)). Use of the 30-wt.% solution in place of the 15-wt.% solution should double the CO_2–MEA reaction rate as discussed in the next section. Moreover, the higher viscosity of the 30-wt.% solution causes it to flow down the wire more slowly, yielding a longer residence time in the test column for fixed $\dot{V}_L$ (see Fig. 3). However, $\dot{M}$ only increases by 30–50%, thereby leading to a decrease in E.

3. Model analysis of chemical gas-absorption

3.1. Outline of the model

The analytic model described here is generally applicable to predicting the rate of absorption of any species initially mixed in a gas phase by a chemically reactive liquid flowing down a wire. For simplicity, however, the gas species and liquid are considered to be CO_2 and an MEA solution, respectively, in the description below so as to be consistent with the experiments described in the preceding section.

The present model was constructed by extending our previous model of physical absorption by a liquid flowing down a wire [2] to consider the CO_2–MEA reaction in the liquid, while the previous model was in turn based on the mechanistic modeling of string-of-beads flow that was reported even earlier from our laboratory with the proposition of applying such flow to gas-to-liquid heat-transfer operations [1]. For the sake of readers' understanding, the present chemical absorption model will be fully described without omitting the portions overlapping the descriptions given in the preceding papers [1,2]. Such portions will be outlined, sometimes referring to related, more detailed descriptions in the preceding papers, while the other portions relevant to the aspects particular to the present chemical-absorption model will be described in more detail.

3.2. Basic assumptions

The basic assumptions used to formulate the string-of-beads flow of, and the CO_2 absorption by, an MEA solution are listed below. They are essentially the same

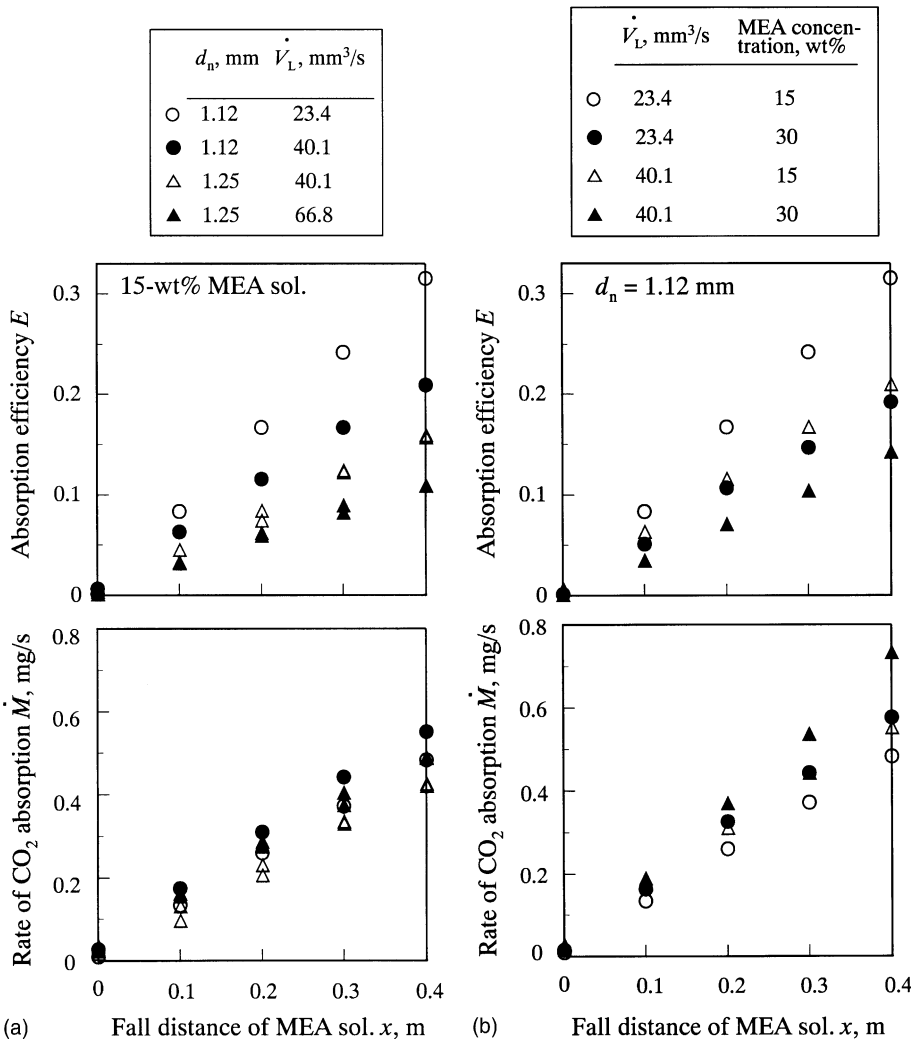

Fig. 4. Summarized results of CO_2 absorption experiments: rate of CO_2 transfer $\dot{M}$ and liquid-side CO_2-transfer efficiency E versus fall distance x of MEA solutions. (a) Variations in CO_2-absorption into 15-wt.% MEA solution with its flow rate and nozzle diameter. (b) Comparison of results obtained with 15- and 30-wt.% MEA solutions.

as those used in the physical absorption modeling [2] except for assumptions (5) and (6).

(1) The films and the beads on a wire are monosized cylinders (diameter, d_f) and spheres (diameter, d_d), respectively, being coaxial and aligned on the wire at uniform intervals.
(2) The fall velocity of the beads, U_d, and the flow velocity in each film averaged over its cross section, U_f, are constant while falling on the wire.
(3) Because $U_d \gg U_f$, each bead continuously engulfs the film ahead of itself and, while simultaneously developing another film at its rear such that the film initially has the same mixed-mean concentration of CO_2 as that in the bead.
(4) The liquid-side CO_2 concentration at the gas–liquid interface, i.e., the surfaces of the films and the beads, is held at c_s, the physical solubility of CO_2 in the MEA solution under the partial pressure of CO_2 in the surrounding gas flow. The partial pressure of CO_2 is assumed to be constant throughout the gas-flow field.
(5) The coefficient of CO_2 transfer inside each film, β_f, is determined by the penetration theory for transient, one-dimensional mass transfer with a first-order chemical reaction [15]. Axial diffusion of CO_2 in the films is neglected.
(6) The coefficient of CO_2 transfer inside each bead, β_d, is determined by the modified Kronig–Brink solution [16] for asymptotic mass transfer inside a fluid

sphere with toroidal internal circulation and a first-order chemical reaction.

(7) The physical properties of the liquid are held constant over the entire gas–liquid contact section irrespective of the spatial variation in the composition of the liquid due to its absorption of CO_2.

Although the physical absorption model [2] safely assumed negligible diffusional resistance in the gas flow compared to that in liquid flow (assumption (4)), this may be an error source because, due to the effect of the CO_2–MEA reaction, the resistance in the MEA solution is substantially lower than that in a non-reactive absorbent such as pure water. The accuracy of using assumption (4) is accordingly evaluated (Section 3.6).

The physical view of CO_2 transfer inside cylindrical films (assumption (5)) is completely different from the assumption of a radially developed CO_2-concentration profile in the previous physical-absorption model [2]. Considering the sufficiently high chemical CO_2-absorption capacity of a 15–30 wt.% MEA solution, it is expected that the penetration theory can safely be used over the period of film-reforming cycle, τ_{fg}, which is close to, though not generally equal to, the interval τ of successive falling beads [1].

The assumption of a toroidal circulation developed inside each bead (assumption (6)) is based on the idea that the bead *rolls down* the wire against the friction exerted at the wire surface. Mechanistic reasoning of the applicability of the Kronig–Brink solution to estimating the heat or mass transfer inside such beads is given elsewhere [1]. As far as the in-bead mass transfer is concerned, the only difference of the present model from the previous physical-absorption model [2] is the introduction of Danckwerts' extension of the Kronig–Brink solution [16] to account for the CO_2–MEA reaction.

Assumption (7) is surmised to be reasonably accurate because the axial change in liquid composition in the gas–liquid contact section is expected to be insignificant.

3.3. Formulation

3.3.1. CO_2–MEA reaction

The overall reaction occurring in the liquid phase over a short time period, such as the residence time of the MEA solutions in the test column, may be expressed as [17]

$$CO_2 + 2RNH_2 \rightarrow RNH_3^+ + RNHCOO^- \tag{3}$$

where R indicates $HCOH_2CH_2$. This reaction is second order, i.e., first order with respect to CO_2 and MEA separately [14], and thus the reaction rate r, being defined as the molar rate of loss of CO_2 per unit volume, is expressed in terms of a reaction rate constant k and molar concentrations of CO_2 and MEA, $\tilde{c}$ and $\widetilde{C}$, as follows:

$$r = k\tilde{c}\widetilde{C}. \tag{4}$$

k can be calculated, using the empirical correlation given by Hikita et al. [14]. Its value corresponding to our experimental conditions is given in Table 1.

As $\widetilde{C}$ is three orders higher than the highest value of $\tilde{c}$, i.e., the molar physical solubility of CO_2 in the employed MEA solution, it is reasonable to assume that $\widetilde{C}$ remains constant at its initial value $\widetilde{C}_0$, the MEA concentration in the 15- or 30-wt.% MEA solution free from CO_2, in each CO_2-absorption experiment, unless the exact mass balance for each species, CO_2 or MEA, is of concern. This assumption allows us to consider the CO_2–MEA reaction as a first-order reaction and to rewrite Eq. (4) as follow:

$$r = k'\tilde{c}, \tag{5}$$

where k' is the reaction rate constant defined as $k\widetilde{C}_0$. This approximate expression for r is used in formulating the mass transfer coefficients in Section 3.3.2, but it is not used in formulating the mass balance for each species in Section 3.3.3.

3.3.2. Mass transfer coefficients

The CO_2 mass transfer into each film is represented by respectively applying the penetration theory to infinitesimal slices of the film which are assumed to fall at a constant velocity U_f like interlinked solid bodies. Based on assumption (4) and Danckwerts' analysis of uni-directional diffusion with a first-order chemical reaction [15], the instantaneous coefficient β_f for mass transfer from the surface into the bulk of an infinitesimal slice is given as a function of time t after the exposure of the surface to the gas mixture as follows [15]:

$$\beta_f = \sqrt{Dk'}\left[\operatorname{erf}\sqrt{k't} + \frac{\exp(-k't)}{\sqrt{\pi k't}}\right]. \tag{6}$$

In the present CO_2–MEA-solution system, k' is of the order of 10^4 s^{-1}; hence, $k't$ is sufficiently large such that we can safely assume that β_f is constant throughout the entire *life* of the slice and is given by

$$\beta_f = \sqrt{Dk'}. \tag{7}$$

Based on assumptions (4) and (6), the CO_2 mass transfer into each bead can be expressed by Danckwerts' expression for the rate of mass transfer into a spherical drop with surface saturation [16]. The expression may be rewritten in a dimensionless form as [18]

$$Sh_d \equiv \frac{\beta_d d_d}{D} = 4\sum_{n=1}^{\infty} A_n^2 \lambda_n \frac{K_R + 16\lambda_n \exp[-\tau_d(K_R + 16\lambda_n)]}{K_R + 16\lambda_n}, \tag{8}$$

where K_R is the dimensionless first-order reaction constant defined as

$$K_R = \frac{k' d_d^2}{4D},$$

τ_d is a dimensionless form of time t after the inception of CO_2 transfer into the bead, i.e., the Fourier number for CO_2 mass diffusion, being defined as

$$\tau_d = \frac{4Dt}{d_d^2},$$

and A_n and λ_n are dimensionless constants. The asymptotic value of Sh_d (the value at $\tau_d \to \infty$) can be obtained by (i) substituting into Eq. (6) the numerical values of A_n and λ_n given in Heertjes et al. [19] for the first seven terms of the series and neglecting the higher-order terms, and (ii) specifying values of $\widetilde{C}_0$ and d_d to be consistent with the CO_2-absorption experiments. Typical asymptotic values thus obtained are higher than that of the original Kronig–Brink solution for non-reactive systems (17.66) by a factor of five or higher.

3.3.3. Mass balance equations

The mass balance for CO_2 and that for MEA is successively formulated for each film element and bead. The balance for CO_2 on a film element, i.e., a slice of an infinitesimal axial thickness, falling at a constant velocity U_f is written as

$$S_f \frac{d\tilde{c}_f}{dt} = \pi d_f \beta_f (\tilde{c}_s - \tilde{c}_f) - S_f k \tilde{c}_f \widetilde{C}_f, \tag{9}$$

where S_f is the cross-sectional area of the film given by

$$S_f = \frac{\pi}{4}\left(d_f^2 - d_w^2\right),$$

$\tilde{c}_f$ and $\widetilde{C}_f$ are the molar, mixed-mean concentrations of CO_2 and MEA, respectively, at an arbitrary axial location designated by x—the axial, downward coordinate with its origin at the nozzle tip—and $\tilde{c}_s$ is the physical solubility of CO_2 in the MEA solution expressed in terms of moles per unit volume. Although $\tilde{c}_s$ should slightly vary with the progression of the CO_2–MEA reaction in the solution, for simplicity we assume that it stays at its initial value in the solution. Because $\tilde{c}_s \gg \tilde{c}_f$ in the considered system, we also assume that the driving force for CO_2 diffusion into the film, $(\tilde{c}_s - \tilde{c}_f)$ in Eq. (9), can be approximated by $\tilde{c}_s$.

To be consistent with Eq. (9), the mass balance for MEA on any, axially thin film-element may be written as

$$\frac{d\widetilde{C}_f}{dt} = -2k\tilde{c}_f \widetilde{C}_f. \tag{10}$$

To formulate the mass balance for each species in a bead, we need to take into account the advective supply of the species into the bead from the film ahead of the bead, which is dependent on the differences in the fall velocity and the species concentration between the bead and film. The balance for CO_2 is written as

$$V_d \frac{d\tilde{c}_d}{dt} = A_d \beta_d (\tilde{c}_s - \tilde{c}_d) + S_f (U_d - U_f)(\tilde{c}_f - \tilde{c}_d) - k\tilde{c}_d \widetilde{C}_d, \tag{11}$$

where V_d and A_d are the volume and surface area, respectively, of the bead, being defined as

$$V_d = \pi\left(\frac{d_d^3}{6} - \frac{d_d d_w^2}{4}\right), \tag{12}$$

$$A_d = \pi\left(d_d^2 - \frac{d_f^2}{2}\right), \tag{13}$$

and $\tilde{c}_d$ and $\widetilde{C}_d$ are the molar concentrations of CO_2 and MEA, respectively, in the bead. Here we assume that $\tilde{c}_d$ and $\widetilde{C}_d$ in Eq. (11) are functions of x at the front of the bead where the film with the mixed-mean CO_2 and MEA concentrations, $\tilde{c}_f$ and $\widetilde{C}_f$, is being merged into the bead. Using similar reasoning as that for considering CO_2 diffusion into the film, the driving force for CO_2 diffusion into the bead, $(\tilde{c}_s - \tilde{c}_d)$, may be replaced by $\tilde{c}_s$.

The mass balance for MEA in a bead is given by

$$V_d \frac{d\widetilde{C}_d}{dt} = S_f (U_d - U_f)(\widetilde{C}_f - \widetilde{C}_d) - 2k\tilde{c}_d \widetilde{C}_d. \tag{14}$$

3.4. Numerical solution procedure

The presented mathematical relations are incorporated into an iterative solution procedure to elucidate how the mass of CO_2 absorbed into the MEA solution per its unit volume, $\hat{c}$, changes with respect to the fall distance of the MEA solution, x. This procedure is not described fully because it is essentially the same as the one described by Chinju et al. [2] for calculating the variation in x of the CO_2 concentration in water, a physical absorbent, flowing down a wire. Only the additional complexity caused by replacing the physical absorption using water by the chemical absorption using an MEA solution will be described below. (Full details of the procedure used in the present study are described by Uchiyama [4].)

The only complexity relevant to the chemical absorption is due to the coupling between the CO_2 concentrations, $\tilde{c}_f$ and $\tilde{c}_d$, and the MEA concentrations, $\widetilde{C}_f$ and $\widetilde{C}_d$. This, however, is not difficult to treat since the resulting problem can be solved by applying an iterative solution procedure simultaneously to $\tilde{c}_f$, $\tilde{c}_d$, $\widetilde{C}_f$, and $\widetilde{C}_d$ to determine their variations with respect to x. The iterative solution procedure itself is analogous to the one used in the preceding physical-absorption study [2]. Once $\tilde{c}_f(x)$, $\tilde{c}_d(x)$, $\widetilde{C}_f(x)$, and $\widetilde{C}_d(x)$ are determined, the time-averaged mixed-mean concentration of MEA at each location on the x axis, $\widetilde{C}_L(x)$, can be calculated as

$$\widetilde{C}_L(x) = \frac{\widetilde{C}_f(x) S_f U_f + \widetilde{C}_d(x) V_d/\tau}{S_f U_f + V_d/\tau}, \tag{15}$$

where U_f is the average flow velocity in a film, being estimated by a fully-developed, annular creeping-flow model [1] as follows:

$$U_f = \frac{g d_w^2}{32 \nu_L}\left(1 - 3a^2 + 4\frac{a^4 \ln a}{a^2 - 1}\right), \tag{16}$$

where g is the acceleration due to gravity, ν_L is the kinematic viscosity of the MEA solution, and $a \equiv d_f/d_w$.

Neglecting the amount of CO_2 physically dissolved in the MEA solution passing any x-axial location compared to the amount of CO_2 that has reacted with the MEA solution prior to arriving at the location, $\hat{c}(x)$ is calculated from $\widetilde{C}_L(x)$ as

$$\hat{c}(x) = \frac{\widetilde{M}}{2}\left[\widetilde{C}_0 - \widetilde{C}_L(x)\right], \tag{17}$$

where $\widetilde{C}_0$ is the initial molar concentration of MEA in the solution and $\widetilde{M}$ the molar mass of CO_2.

3.5. Calculation results

By specifying the experimental conditions—d_w, $\dot{V}_L$, and the physical properties of the MEA solution and of CO_2/MEA-solution binary system—and by substituting relevant observed values into d_f, d_d (approximated by $(d_{d1}d_{d2}^2)^{1/3}$), U_d and τ, we can compute $\hat{c}(x)$ and subsequently predict $E(x)$, the transfer efficiency defined by Eq. (2) in which $\hat{c}_{out}$ and $\hat{c}_{in}$ should be read as $\hat{c}(x)$ and zero, respectively. The results thus obtained are exemplified in Fig. 5 together with corresponding experimental results. The agreement between the predictions and relevant experimental data is generally good. This fact indicates the practical utility of the chemical absorption model described above in predicting actual gas-absorption performance of on-wire liquid-absorbent flow operations, using only empirical knowledge of on-wire flow dynamics.

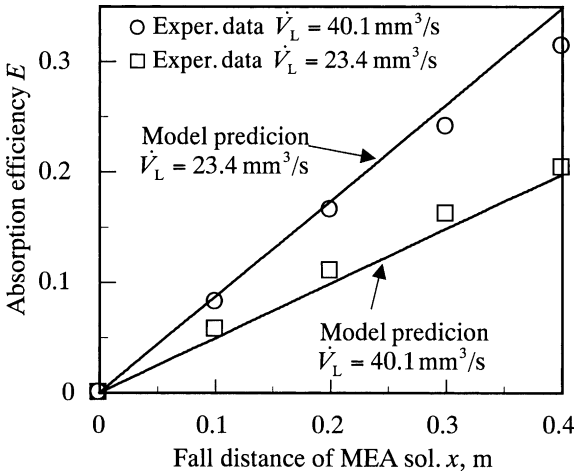

Fig. 5. Comparison of predicted absorption efficiency with corresponding experimental data. $d_n = 1.12$ mm.

3.6. Diffusional resistance in gas flow

One assumption affecting the validity of the present chemical-absorption model is whether or not diffusional resistance in the gas flow is negligible. This resistance was accordingly evaluated by performing a numerical analysis of convective mass transfer from the gas flow to the surface of a liquid in string-of-beads flow.

3.7. Modeling and numerical solution procedure

Let us assume a steady, axisymmetric gas flow bordered by two concentrically arranged walls, say wall A and B. As illustrated in Fig. 6, wall A patterns the contour of the liquid/gas interface observed in an experiment in which the 15-wt.% MEA solution was released from the larger nozzle ($d_n = 1.25$ mm) at the highest flow rate ($\dot{V}_L = 66.8$ mm^3/s). This wall is composed of bead- and film-shaped portions alternately aligned along the axis of symmetry. These two portions axially move at different velocities; the bead-shaped portions move at 315 mm/s (= U_d measured in the experiment) and the film portions move in the same direction at 12.8 mm/s (= U_f calculated by Eq. (16)). Wall B, concentric with wall A, is the outer boundary of the gas-flow field, being 103 mm away from their common axis such that its presence does not affect the flow around, and the mass transfer to, wall A. The same CO_2/N_2 mixture as that used in the experiments flows through the annular space between the two walls in the direction opposite to the motion of wall A. As in the experiments, the superficial velocity of the gas mixture is 31.8 mm/s. *No-slip* and *slip* conditions are imposed on wall A and B, respectively. Both walls extend 300 mm along the x coordinate. The gas mixture with a uniform flow velocity and a uniform composition (0.1 CO_2 mole fraction) enters the annular space at one end ($x = 300$ mm) and flows out at the other end ($x = 0$). The physical properties of the gas mixture are evaluated at a temperature of 25 °C under atmospheric pressure, being consistent with the experiments. The CO_2 concentration on wall A is assumed to be constant.

The problem posed above constitutes an unsteady, moving-boundary problem due to the axial motion of wall A having an axially periodical configuration. A commercial general-use solver, FLUENT (Version 4.38, Fluent Inc.), was utilized to solve the convective-heat transfer problem analogous to the mass transfer problem posed above. To well simulate spatial variations in flow and temperature (corresponding to CO_2 concentration) near the front side of each bead-shaped portion of wall A, such a non-uniform grid as the one illustrated in Fig. 6 was laid on the gas-flow field. The local heat

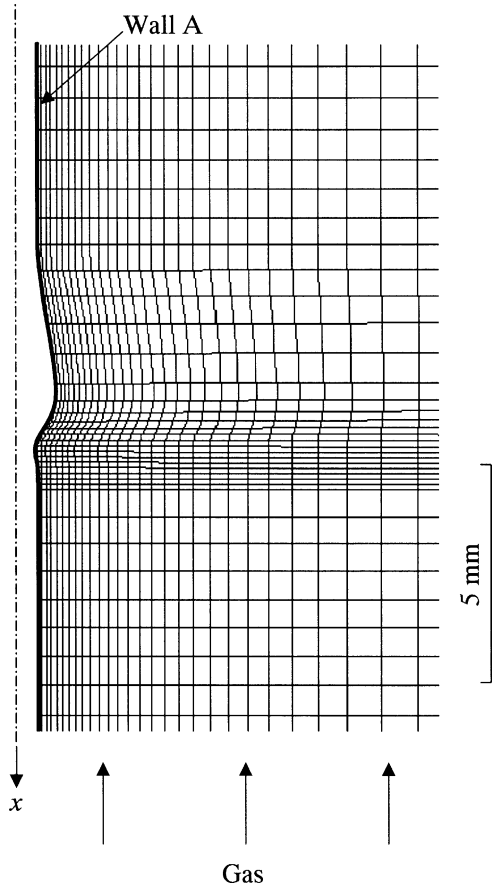

Fig. 6. Graphical representation of a small portion of the gas-flow field modeled for numerical simulation of forced-convective CO_2 transfer to the liquid-absorbent surface patterned by wall A. Wall B (not shown) is located at 103 mm radially outward from the central axis. Fine reticulated lines illustrate the grid laid on the gas-flow field for numerical solution procedure. Irregular breaks of some of the lines are due to an insufficient graphic function of the employed commercial solver (FLUENT, Ver. 4.38).

transfer coefficient on wall A thus determined was readily converted to the local mass transfer coefficient for CO_2, $\beta_G(x)$.

3.8. Results of simulation: the resistance in gas flow

It was confirmed that $\beta_G(x)$ exhibits periodic variation with x in synchronism with alternations of the bead- and film-shaped portions along the x axis. Fig. 7 shows the axial variation of the reciprocal of $\beta_G(x)$—the diffusional resistance in the gas phase, R_G—over a small, arbitrarily selected part of the entire x range ($0 \leqslant x \leqslant 300$ mm) over which the simulation was made. It is interesting to note that R_G sharply increases and decreases in the gas flow direction, i.e., the direction of decreasing x,

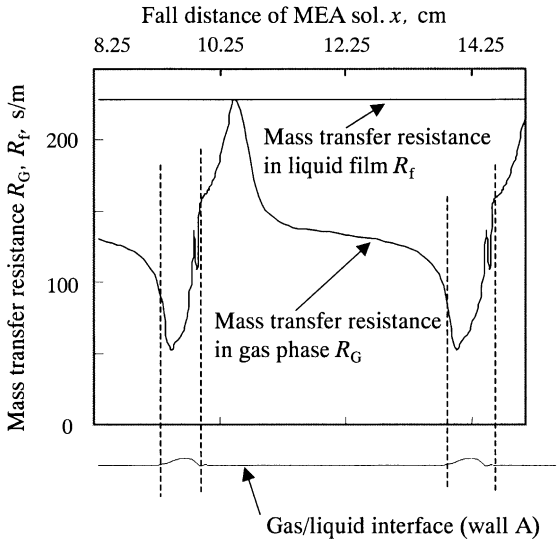

Fig. 7. Resistance to CO_2 transfer in gas phase compared with that in liquid films for the 15-wt.% MEA solution.

within a relatively short axial length on the downstream side of the film-shaped portion. This behavior is due to the axial variation in the concentration boundary-layer thickness over the film-shaped portion under the influence of the bead-shaped portion oncoming from the downstream side.

Also shown for comparison in Fig. 7 is R_f, the diffusional resistance in liquid films evaluated as the reciprocal of β_f given by Eq. (7). Since the resistance in liquid beads inferred by the asymptotic value of β_d given by Eq. (8) is higher than R_f by two orders, it is not shown. Such comparative evaluations of element resistances to CO_2 transfer indicate that the resistance in the gas phase is generally less significant than that in the liquid phase, although not necessarily negligible. In fact, as the peak value of R_G is comparable to R_f, it becomes apparent that assuming negligible resistance in the gas phase is not very accurate under the conditions set in the CO_2-absorption experiments. Consequently, the analytic model described in Sections 3.1–3.3 might have overestimated the CO_2-absorption performance to some extent due to assuming negligible gas-phase resistance. The good agreement between calculational and experimental results for CO_2-absorption performance (Fig. 5) may be partially due to a fortunate offset of the error caused by the above assumption to those resulting from other assumptions and/or simplifications used in the model. The refinement of the model is left for future study.

4. Conclusions

This paper has presented the first attempt of applying string-of-beads flow to the operations of chemical ab-

sorption for separating a gaseous species. The model experiments using MEA solutions as the liquid absorbent flowing down a single wire vertically hung in a counterflowing CO_2/N_2 mixture have revealed the operational parameters that control gas-absorption performance of the string-of-beads flow. The results of the experiments indicate that the nozzle/wire assembly and concentration of MEA should be properly adjusted to meet the requirements for, for example, the rate of absorption and the absorption efficiency at a prescribed height of the gas–liquid contact section.

A model analysis is also presented to provide (i) a mechanistic and physicochemical interpretation of the experimental results, and (ii) a means to predict the gas-absorption performance at arbitrary adjustments of operational parameters such as the chemical species of the absorbent, flow rate of the absorbent on each wire, height of the gas–liquid contactor, and space assigned to each wire in the contactor. Reasonably good agreement between predictions by the model and corresponding experimental results supports the general validity of the physical view underlying the model. Although there is still room for further refinement, the model nevertheless can be used as is to quantitatively estimate how absorption performance varies with operational parameters. In fact, we expect it to have application potential as a prototype design tool for developing *wetted-wire columns* for use in chemical absorption operations.

Acknowledgements

This study was supported by a research grant from the Iwatani Naoji Foundation and by a Grant-in-Aid for Scientific Research from the Japan Society for the Promotion of Science (grant no. 13450087). We extend our sincere gratitude to Prof. Shuichi Matsumura, Dept. of Applied Chemistry, Keio University, for his kind supervision regarding the employed precipitation-titration method.

Appendix A. Measurements of bead length

Because each bead has a teardrop shape with a slender rear that smoothly merges with a cylindrical film, its trailing edge is not very clear. (The actual bead profile may be recognized in the photographs given by Chinju et al. [2]; also the profile is accurately represented by "wall A" in Fig. 6.) Thus, we now describe how we determined the location of the trailing edge of the bead and how to measured its axial length, d_{d1}.

All of the video-image analysis works in the present study were performed using a non-commercial image-analysis software, PIMg2G [20]. The videographs of the MEA solutions in string-of-beads flow were stored in a digital memory in the form of 640×480 pixel images, which were then converted into binary (black and white) images. These images were processed to yield digitized data of the string-of-beads profile. Thus, every dimensional measurement related to the string-of-beads profile is inevitably accompanied by an uncertainty of the order of the size of one pixel in a video image, which corresponds to $\sim$13 μm. The trailing edge of each bead was defined as the axial location where the diameter of the bead approaches that of the film within one pixel. The leading edge of the bead was defined as the location where the cylindrical film ahead of the bead was constricted to yield the minimum diameter of the liquid/gas interface (see Fig. 6). The difference in the axial coordinate between the leading and trailing edges of the bead was recorded as its axial length, d_{d1}.

References

[1] K. Hattori, M. Ishikawa, Y.H. Mori, Strings of liquid beads for gas–liquid contact operations, AIChE J. 40 (1994) 1983–1992.
[2] H. Chinju, K. Uchiyama, Y.H. Mori, "String-of-beads" flow of liquids on vertical wires for gas absorption, AIChE J. 46 (2000) 937–945.
[3] F.-Y. Jou, A.E. Mather, F.D. Otto, The solubility of CO_2 in a 30 mass percent monoethanolamine solution, Can. J. Chem. Eng. 73 (1995) 140–147.
[4] K. Uchiyama, Application of "strings-of-beads" liquid flow to gas absorption, M.Sc thesis, Keio University, Yokohama, Japan, 1999.
[5] J.-H. Song, S.-B. Park, J.-H. Yoon, H. Lee, Densities and viscosities of monoethanolamine + ethylene glycol + water, J. Chem. Eng. Data 41 (1996) 1152–1154.
[6] H. Hikita, H. Ishikawa, K. Uku, T. Murakami, Diffusivities of mono-, di-, and triethanolamines in aqueous solutions, J. Chem. Eng. Data 25 (1980) 324–325.
[7] G. Vázquez, E. Alvarez, J.M. Navaza, R. Rendo, E. Romero, Surface tension of binary mixtures of water + monoethanolamine and water + 2-amino-2-methyl-1-propanol and tertiary mixtures of these amines with water from 25 °C to 50 °C, J. Chem. Eng. Data 42 (1997) 57–59.
[8] S.S. Laddha, P.V. Danckwerts, Reaction of CO_2 with ethanolamines: kinetics from gas-absorption, Chem. Eng. Sci. 36 (1981) 479–482.
[9] G.F. Versteeg, W.P.M. van Swaaij, Solubility and diffusivity of acid gases (CO_2, N_2O) in aqueous alkanolamine solutions, J. Chem. Eng. Data 33 (1988) 29–34.
[10] J.I. Lee, F.D. Otto, A.E. Mather, Equilibrium between carbon dioxide and aqueous monoethanolamine solutions, J. Appl. Chem. Biotechnol. 26 (1976) 541–549.
[11] H.G. Muhlbauer, P.R. Monaghan, Sweetening natural gas with ethanolamine solutions, Oil Gas J. 28 (1957) 139–145.
[12] G.E.H. Joosten, P.V. Danckwerts, Solubility and diffusivity of nitrous oxide in equimolar potassium carbonate-potassium bicarbonate solutions at 25 °C and 1 atm, J. Chem. Eng. Data 17 (1972) 452–455.

[13] E. Sada, H. Kumazawa, M.A. Butt, Solubility and diffusivity of gases in aqueous solutions of amines, J. Chem. Eng. Data 23 (1978) 161–163.
[14] H. Hikita, S. Asai, Y. Katsu, S. Ikuno, Absorption of carbon dioxide into aqueous monoethanolamine solutions, AIChE J. 25 (1979) 793–800.
[15] P.V. Danckwerts, Absorption by simultaneous diffusion and chemical reaction, Trans. Faraday Soc. 46 (1950) 300–304.
[16] P.V. Danckwerts, Absorption by simultaneous diffusion and chemical reaction into particles of various shapes and into falling drops, Trans. Faraday Soc. 47 (1951) 1014–1023.
[17] E. Sada, H. Kumazawa, M.A. Butt, Chemical absorption kinetics over a wide range of contact time: absorption of carbon dioxide into aqueous solutions of monoethanolamine, AIChE J. 22 (1976) 196–198.
[18] H. Watada, A.E. Hamielec, A.I. Johnson, A theoretical study of mass transfer with chemical reaction, Can. J. Chem. Eng. 48 (1970) 255–261.
[19] P.M. Heertjes, W.A. Holve, H. Talsma, Mass transfer between isobutanol and water in a spray-column, Chem. Eng. Sci. 3 (1954) 122–142.
[20] PIMg2G—an image-analysis software, Programmed and provided by K. Ishida, Dept. of Mechanical Engineering, Keio University, Yokohama, Japan, 1998.